Local structure of Mn in hydrogenated $Ga_{1-x}Mn_xAs$

C. Bihler,[1,*] G. Ciatto,[2] H. Huebl,[1] G. Martinez-Criado,[3] P. J. Klar,[4] K. Volz,[5] W. Stolz,[5] W. Schoch,[6] W. Limmer,[6] F. Filippone,[7] A. Amore Bonapasta,[7] and M. S. Brandt[1]

[1]*Walter Schottky Institut, Technische Universität München, Am Coulombwall 3, 85748 Garching, Germany*

[2]*Synchrotron SOLEIL, L'Orme des Merisiers, Saint-Aubin, Boîte Postale 48, 91192 Gif-sur-Yvette Cedex, France*

[3]*Experiments Division, European Synchrotron Radiation Facility, 38043 Grenoble, France*

[4]*Institute of Experimental Physics I, Justus Liebig University, Heinrich-Buff-Ring 16, 35392 Giessen, Germany*

[5]*Department of Physics and Material Sciences Center, Phillipps University, Renthof 5, 35032 Marburg, Germany*

[6]*Institut für Halbleiterphysik, Universität Ulm, 89069 Ulm, Germany*

[7]*CNR, Istituto di Struttura della Materia (ISM), Via Salaria Km 29.5, Cassella Postale 10, 00016 Monterotondo Stazione, Italy*

(Received 18 September 2008; published 31 December 2008)

In this paper we investigate the incorporation of hydrogen in $Ga_{1-x}Mn_xAs$ for samples with $x \approx 0.005$ grown by metal-organic vapor-phase epitaxy and with $0.03 < x < 0.05$ grown by low-temperature molecular-beam epitaxy. The anisotropic electron-paramagnetic-resonance (EPR) signal observed for the paramagnetic $Ga_{1-x}Mn_xAs$ samples with $x \approx 0.005$ after hydrogenation is characteristic for Mn^{2+} substitutional on the Ga site. Contributions of crystal fields to the EPR signal indicative of Mn-H complexes with H atoms near the Mn are negligibly small. The relative volume increase in a single Mn_{Ga}-As atom pair upon hydrogenation $\Delta V_H / V_{Mn\text{-}As} \approx 0.14 \pm 0.07$ as deduced from a comparison of the high-resolution x-ray diffraction $2\Theta/\Omega$ scans of as-grown and hydrogenated samples with $0.03 < x < 0.05$ is expected for Mn-H complex formation. However, the accuracy of this measurement is not sufficient to draw unambiguous conclusions about the specific nature of the Mn-H configuration. Extended x-ray absorption fine-structure (EXAFS) analysis and x-ray absorption near-edge spectroscopy (XANES) on samples with $0.03 < x < 0.05$ show no indication for bond-centered Mn-H complexes as determined from a detailed comparison of the EXAFS Fourier transforms and the XANES spectra with the simulations. The overwhelming structural evidence of these techniques therefore points to comparatively large distances between the Mn and the H atoms at least in $Ga_{1-x}Mn_xAs$ films with Mn concentrations above 0.005, which would be the case for either complexes with the hydrogen atom in the antibonding position or for compensation via isolated interstitial hydrogen.

DOI: 10.1103/PhysRevB.78.235208 PACS number(s): 75.50.Pp, 76.30.Fc, 78.70.Dm, 78.70.Ck

I. INTRODUCTION

Ferromagnetic semiconductors such as $Ga_{1-x}Mn_xAs$ are of interest for applications in spintronics, in particular for the realization of contacts for the injection of spin-polarized charge carriers. In $Ga_{1-x}Mn_xAs$, both the localized magnetic moments as well as the itinerant holes mediating the ferromagnetic coupling between them are introduced by manganese acceptors.[1–3]

Different ways of switching or influencing the magnetism in this material are currently being investigated and summarized in Ref. 4. One possibility is via postgrowth hydrogenation.[5] Upon exposure to a remote dc hydrogen plasma, the conductivity in $Ga_{1-x}Mn_xAs$ films, which is nearly temperature independent (metallic) in their as-grown state, can be reduced by several orders of magnitude without affecting the density of localized Mn magnetic moments.[6–8] This drastic decrease in conductivity is accompanied with a disappearance of the ferromagnetic coupling as expected for carrier-mediated ferromagnetism in this material.[5,9] Recently, a similar behavior upon hydrogenation has also been observed in $Ga_{1-x}Mn_xP$.[10] The decrease in carrier concentration can be explained via a hydrogenation-induced change in the Mn charge state. In the as-grown state Mn with the electron configuration $[Ar]3d^5 4s^2$ substitutes Ga with the electron configuration $[Ar]3d^{10}4s^2 4p^1$, where [Ar] denotes the electron configuration of argon. The acceptor property of Mn follows directly from the difference in the electron configuration and the depth of the Mn acceptor level in the band gap determines the localization of the holes. In the case of $Ga_{1-x}Mn_xAs$, Mn exhibits a shallow acceptor level in the vicinity of the valence-band edge and Mn thus predominantly is present in the $[Mn^{2+}(3d^5)+h^+]^{3+}$ state with a hole h^+ in the valence band. Since hydrogen in $Ga_{1-x}Mn_xAs$ acts as an amphoteric impurity,[11] hydrogenation either leads to a compensation of the Mn acceptors by H donors or to a passivation of the Mn acceptors by the formation of electrically neutral Mn-H complexes. In other words, hydrogenation pushes the Fermi level above the $Mn^{3+/2+}$ charge-transfer level and thus leads to a transition of the Mn atom from the $[Mn^{2+}(3d^5)+h^+]^{3+}$ state to the $Mn^{2+}(3d^5)$ state, removing the acceptor level. The loss of conductivity and the accompanying loss of ferromagnetism upon hydrogenation of $Ga_{1-x}Mn_xAs$ have now been reported by several groups.[5,7–9,12–14] While the fundamental effects of hydrogen on the magnetic properties are therefore established, there are still open questions remaining concerning the local microscopic structure of hydrogen in this material, be it in the form of well-defined acceptor-hydrogen complexes or in the form of isolated donors. This paper addresses this issue using spectroscopic methods.

Secondary ion mass spectrometry (SIMS) measurements of hydrogenated $Ga_{1-x}Mn_xAs$ samples showed that Mn and H concentrations are identical within experimental uncertainty.[8] In the infrared-absorption spectra at 6 K of hy-

drogenated and deuterated samples, absorption maxima at 2143 and 1546 cm^{-1}, respectively, have been attributed to local vibrational As-H and As-D stretching modes and were taken as evidence for the formation of electrically inactive complexes involving manganese and hydrogen.[6–8] The fact that these As-H and As-D stretching modes are very similar to those observed for GaAs doped with other acceptors such as Mg and Zn (compare Table I in Ref. 8), and thus are nearly independent of the specific acceptor considered, was taken as an indication that hydrogen is located in an antibonding configuration in the Mn_{Ga}-H complex. However, although the frequency of the As-H stretching mode is very similar for Mg, Zn, and Mn acceptors, it exhibits a clear increase with the size of the acceptor when compared to the modes in GaAs:Be and GaAs:Cd.[15] This behavior in contrast was taken as an indication that hydrogen is in the close proximity of the acceptor, as it is the case at the bond-centered site in between the acceptor and a neighboring As atom.[15] Also density-functional calculations predict that the H atom in the Mn_{Ga}-H complex energetically favors the bond-centered configuration.[16,17] The local vibrational modes calculated for the bond-centered configuration agree with the experimentally observed values, while for the antibonding site smaller stretching frequencies than observed were predicted theoretically.

Interestingly, the local vibrational mode spectroscopy so far is the only method which has provided structural information concerning Mn-H complexes. The same holds essentially for most dopant-hydrogen complexes in semiconductors in general. Here, we will use two other spectroscopic techniques to address the position of H in as-grown and hydrogenated $Ga_{1-x}Mn_xAs$. One of these techniques relies on the particular charge and spin state of Mn. Both as part of a complex and when compensated, the Mn atoms should be in the $Mn^{2+}(3d^5)$ state with g factor $g=2$ and spin $S=5/2$. As we already showed in a former publication, the paramagnetic magnetization after hydrogenation can indeed be described by a Brillouin function with these parameters.[5] However, the direct observation of electron paramagnetic resonance (EPR) of this Mn^{2+} state would provide direct information on the symmetry of the crystal field of the Mn^{2+} atoms from which information on the position of the H might be inferred. Note that EPR has already been applied to obtain structure-sensitive data, e.g., for the Pt-H_2 complex in Si,[18,19] gold-hydrogen complexes in Si,[20] or the nitrogen-vacancy-hydrogen complex in diamond.[21] These studies are based on the symmetry of the ligand- and hydrogen-related hyperfine structures as well as on the electron localization on the different sites.

The second spectroscopic technique is x-ray absorption fine-structure (XAFS) analysis. Performing XAFS at the absorption edge of the dopant in epitaxial semiconductor epilayers is usually very challenging due to the high dilution and the relatively low thickness of the samples. Nevertheless, on one hand our samples have been grown by a nonstandard low-temperature molecular-beam epitaxy (LT-MBE) technique which yields $Ga_{1-x}Mn_xAs$ epilayers with rather high dopant concentration [up to $x \approx 20\%$ (Ref. 22)], on the other hand, nowadays, third generation synchrotron-radiation sources are able to deliver a very high x-ray flux on the samples. As a consequence of these two facts, high quality XAFS data can be obtained on our samples in a reasonable time. Note that a relatively high Mn concentration (exceeding 1%) is needed to achieve ferromagnetism in GaAs.

In this paper we therefore use these two techniques to investigate the incorporation of hydrogen in $Ga_{1-x}Mn_xAs$ in two different sample series described in Sec. II with $x \approx 0.005$ grown by metal-organic vapor-phase epitaxy (MOVPE) and with $0.03 < x < 0.05$ grown by LT-MBE. In the first part of the paper, we discuss the anisotropic EPR signal observed for the paramagnetic $Ga_{1-x}Mn_xAs$ samples with $x \approx 0.005$ after hydrogenation (Sec. III). Similar anisotropies were already reported by Almeleh and Goldstein[23] as well as Fedorych *et al.*[24] for strongly compensated $Ga_{1-x}Mn_xAs$ samples. In the second part of the paper, we investigate the microscopic structure of hydrogenated $Ga_{1-x}Mn_xAs$ samples with $0.03 < x < 0.05$ by means of high-resolution x-ray diffraction (HR-XRD) and XAFS. We determine the volume increase in a single Mn_{Ga}-As pair upon hydrogenation from a comparison of $2\Theta/\Omega$ scans of as-grown and hydrogenated samples and compare this value with theoretical predictions for several complex configurations (Sec. IV). Furthermore, for the bond-centered complex configuration theory predicts an extension of the accompanying Mn-As distance, resulting in a significant change in the radial distribution function of the Mn atom, which is investigated via XAFS measurements (Secs. V and VI).

II. SAMPLE GROWTH AND HYDROGENATION

The 2 μm thick samples with a Mn content of $x \approx 0.005$ were grown on (001)-oriented semi-insulating GaAs wafers using MOVPE.[25] The characterization of these samples by photoluminescence, Hall effect, SIMS, HR-XRD, and transmission electron microscopy showed that the concentration of manganese interstitials is negligible.[25] Spin-flip Raman spectra taken with the laser excitation close to the band gap revealed that in the as-grown samples all Mn_{Ga} atoms are in the neutral charge state A^0 with a shallow valence-band hole h bound to the negative deep acceptor $(3d^5+h)$ as expected. In particular, no evidence of the compensated A^- charge state $(3d^5)$ was found.[25]

The $Ga_{1-x}Mn_xAs$ thin films (thickness 175 nm $< d <$ 260 nm) with higher Mn concentration $(0.03 < x < 0.05)$ were grown by LT-MBE in a RIBER 32 system on In-mounted semi-insulating GaAs(001) substrates. The nominal Mn concentration x was determined from Mn and Ga flux measurements. More details on the LT-MBE growth can be found in Ref. 26.

The hydrogenation was carried out via a remote dc deuterium plasma operated at 0.9 mbar, with the sample heated to 170 °C. To ensure complete hydrogenation we exposed the samples to the plasma for 168 h. Annealed control samples were prepared in the same way, but with the hydrogen plasma switched off to study the influence of the temperature on the treatment. LT-MBE samples demonstrate the published behavior, in particular a full suppression of the ferromagnetism in superconducting quantum interference device (SQUID) magnetometry measurements,[5,7] a reduction in

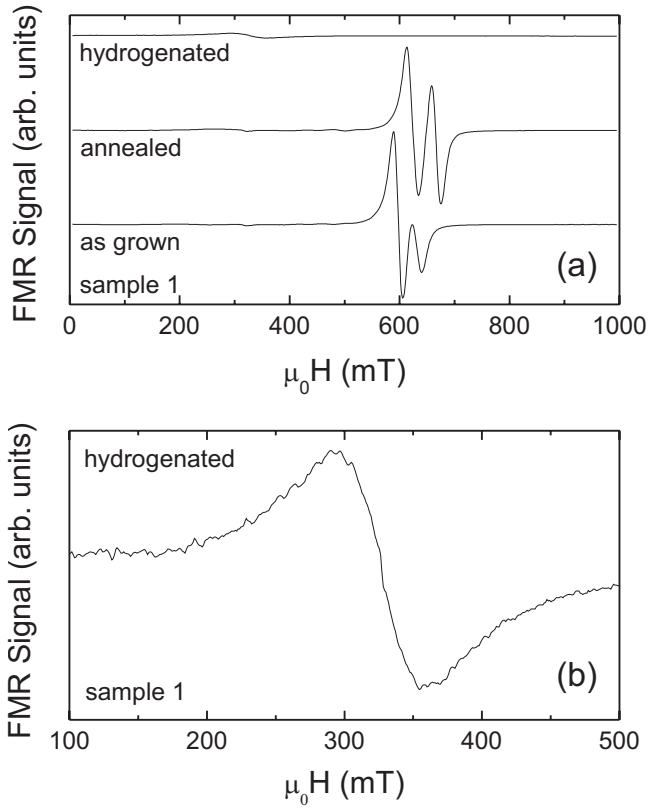

FIG. 1. (a) Ferromagnetic resonance spectra of the as-grown, the annealed, and the hydrogenated sample 1 investigated via XAFS in Sec. V for the external magnetic field oriented perpendicular to the film plane at 5 K. Hydrogenation leads to a strong suppression of the ferromagnetic resonance signal. The hydrogenated sample features a broad paramagnetic resonance at $g=2.0$ scaled up in (b).

the conductivity,[5,8] and the appearance of a local vibrational mode at 1546 cm^{-1} (note that we used the isotope deuterium) via Fourier-transform infrared spectroscopy.[8] Furthermore, in Fig. 1 we show the characterization of sample 1 investigated by XAFS in Sec. V by ferromagentic resonance (FMR) spectroscopy. At the microwave frequency $\omega/(2\pi)=9.3$ GHz paramagnetic impurities with a g factor $g=2$ yield a paramagnetic resonance at the external magnetic field $\mu_0 H=\hbar\omega/(g\mu_B)=330$ mT, where μ_0 is the vacuum permeability, $\hbar$ is the reduced Planck constant, and μ_B is the Bohr magneton. For ferromagnetically coupled magnetic moments, magnetic anisotropy leads to a shift of the ferromagnetic resonance field to $\mu_0 H>330$ mT ($\mu_0 H<330$ mT) if the external magnetic field is oriented along a magnetic hard (easy) axis.[27] For the external magnetic field aligned along growth direction the as-grown sample shows a FMR at $\mu_0 H\approx 600$ mT [Fig. 1(a)] which is due to a uniaxial magnetic anisotropy with a magnetic hard axis in growth direction caused by epitaxial strain. The double-resonance structure we attribute to the presence of a gradient in the magnetic properties.[28,29] Upon annealing the FMR shifts to larger $\mu_0 H$, consistent with an increase in hole concentration and the accompanied increase in the uniaxial anisotropy in growth direction.[12] As expected, the hydrogenated sample does not show a FMR, but a paramagentic resonance at 330 mT corresponding to $g=2$. The peak-to-peak linewidth $\mu_0 H_{\mathrm{p.p.}}\approx 68$ mT of this paramagnetic resonance is consistent with the total width of the resolved hyperfine split multiline spectrum of Mn^{2+} discussed for the hydrogenated MOVPE samples in Sec. III. The signal intensity of the resonance in Fig. 1(b) yields a total number of Mn^{2+} of $\approx 10^{15}$ for the particular piece of sample investigated, which is in reasonable agreement with the total number of Mn atoms of 2.4×10^{15} derived from the growth parameters.

As discussed in Sec. III, the initially paramagnetic MOVPE samples ($x\approx 0.005$) stay paramagnetic upon hydrogenation. No local vibrational modes could be observed for the hydrogenated MOVPE samples. However, the appearance of an anisotropic electron-paramagnetic-resonance signal of the $Mn^{2+}(3d^5)$ state in the samples after exposure to the plasma—as discussed below—indicates the successful incorporation of hydrogen.

III. EPR

EPR is an established experimental technique that is used to identify defects via the symmetry of their localized paramagnetic states. For our investigations we used a commercial EPR system at 9.3 GHz with magnetic field modulation. All EPR measurements were performed at $T=5$ K using a liquid-He flow cryostat. The samples investigated in this section exhibit a Mn concentration of $x\approx 0.005$. As discussed by Schneider *et al.*,[30] the A^0 (Mn^{3+}) and A^- (Mn^{2+}) charge states of Mn in GaAs can be identified in EPR via their different g factors of $g=2.77$ and $g=2.00$, respectively. In EPR measurements of our samples in their as-grown state, neither a signal of the A^0 nor one of the A^- charge state could be detected. A reason could be a higher susceptibility of the EPR of the A^0 state to strain compared to the A^- state.[31] Note that the Mn concentration $x\approx 0.005$ of our ≈ 2 μm thick MOVPE samples is about 3 orders of magnitude larger than the Mn concentration of the samples cut from a GaAs:Mn ingot doped in the melt studied in Ref. 30. Therefore, epitaxial strain in our samples is the likely origin for the failure to observe the A^0 state in EPR of the as-grown samples.

After hydrogenation, the two samples investigated both showed identical resonances at 305 mT $<\mu_0 H<$ 355 mT in EPR. The spectra for a rotation of the external magnetic field in the $(\bar{1}10)$ crystal plane in steps of 10° are shown in the bottom part of Fig. 2. φ is the angle between the growth direction [001] and the magnetic field direction. The anisotropy observed is characteristic for $Mn^{2+}(3d^5)$ ions with $g=2$ and $S=5/2$.[23,24] At $\varphi=30°$ and $\varphi=90°$ a resolved hyperfine structure consisting of six resonances can be observed. The spectra and their anisotropy can be understood by means of the Breit-Rabi diagram shown in Fig. 3. The electronic Zeeman interaction described by g causes a splitting into six levels with the magnetic quantum number $m_s=-5/2,-3/2,-1/2,\ldots,5/2$, which are equally spaced at high magnetic fields. This degeneracy in level spacing is lifted by the influence of the crystal field, resulting in a fine-structure splitting. Furthermore, each Zeeman level is split sixfold by the hyperfine interaction with the nuclear spin $I=5/2$ of the ^{55}Mn nuclei. Consequently, between neighboring electronic Zeeman levels ($\Delta m_s=\pm 1$) there are six allowed magnetic-dipole

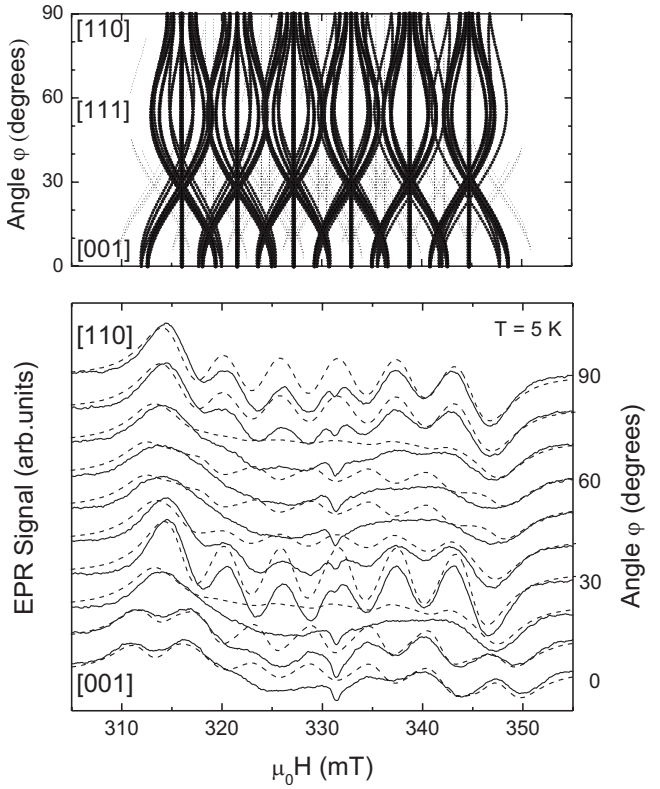

FIG. 2. The upper diagram shows the anisotropy of the EPR resonance fields $\mu_0 H_{\mathrm{res}}$ simulated using $g=2$, $A=-5.75$ mT$\times g\mu_B$, $D_{001}=-0.1$ mT$\times g\mu_B$, $D_{111}=0.1$ mT$\times g\mu_B$, and $a=-1.55$ mT$\times g\mu_B$. The size of the dots corresponds to the expected intensity of the respective resonance line. The lower diagram shows the angular dependence of the EPR of the hydrogenated MOVPE-grown sample with $x\approx 0.005$ (full lines). The spectra have been simulated (dashed line) with the same parameters as in the upper diagram.

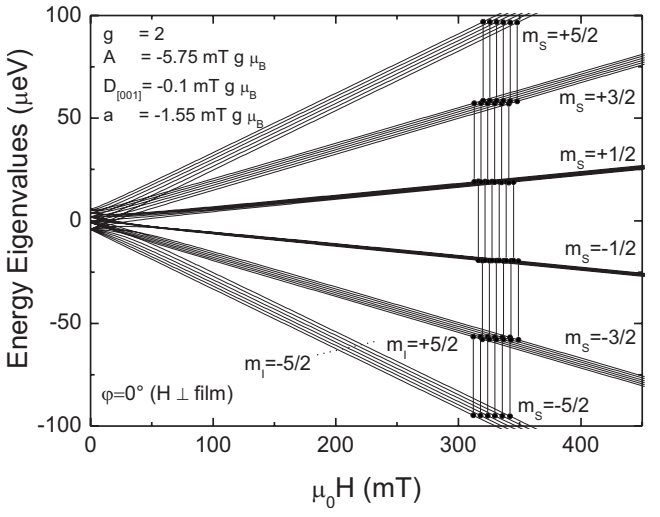

FIG. 3. Breit-Rabi diagram for GaAs:Mn^{2+} with the magnetic field oriented normal to the $Ga_{1-x}Mn_xAs$ layer. The vertical lines indicate the allowed magnetic-dipole transitions with $\Delta m_s=\pm 1$ and $\Delta m_i=0$ for a transition energy of 39 μeV corresponding to a microwave frequency of 9.3 GHz.

transitions with $\Delta m_i=0$ observable via EPR, giving rise to a total of 30 resonance lines expected in the EPR spectra (m_i denotes the quantum number of the nuclear spin). If—as in the sample investigated—the fine-structure splitting is smaller than the hyperfine splitting, the five fine-structure line groups will overlap and thus diminish the resolution of the hyperfine resonances. In this case, only for orientations of the external magnetic field exhibiting negligible fine-structure splitting, the six hyperfine resonances will be resolved which in our sample is the case at $\varphi=30°$ and $\varphi=90°$ orientations.

To analyze the experimental data in detail we use the spin Hamiltonian,

$$\mathcal{H}_S = g\mu_B\mu_0\vec{H}\vec{S} + A\vec{S}\vec{I} + D_{001}\left[S_z^2 - \frac{1}{3}S(S+1)\right] + 2D_{111}[\pm S_xS_y \pm S_yS_z \pm S_zS_x] + \frac{1}{6}a\left[S_x^4 + S_y^4 + S_z^4 - \frac{1}{5}S(S+1)(3S^2+3S-1)\right]. \quad (1)$$

The first term is the electronic Zeeman interaction. The second term describes the hyperfine interaction, which is assumed to be isotropic with the hyperfine constant A. $\vec{S}$ and $\vec{I}$ are the electronic and nuclear-spin operators. The last three terms with D_{001}, D_{111}, and a describe the fine-structure interaction of the electronic spin S with the crystal field, accounting for the particular anisotropies. As shown schematically in Fig. 4(b) there is on one hand a uniaxial crystal-field anisotropy contribution D_{001} caused by the pseudomorphic growth of the $Ga_{1-x}Mn_xAs$ layer. The latter leads to a larger lattice constant c in growth direction compared to the in-plane lattice constant a_{GaAs}, which equals the lattice constant of the GaAs substrate (cf. Sec. IV). On the other hand, the incorporation of hydrogen is expected to lead to a uniaxial crystal-field anisotropy along the $\langle 111\rangle$ directions since both for the bond-centered and the antibonding configurations a reduction in the crystal-field symmetry along the corresponding Mn-As bond axis is expected [Figs. 4(c) and 4(d)]. As we assume that there is only one hydrogen atom per Mn_{Ga}-H complex as suggested by SIMS; we have to distinguish between the four possible $\langle 111\rangle$ directions in $\mathcal{H}_S$, where the terms S_xS_y differ in signs. For each direction the eigenenergies have to be calculated separately increasing the total number of resonances obtained from the simulation to 120. Finally, the last term in Eq. (1) with the parameter a takes into account the cubic symmetry of the GaAs host crystal.

The best fit to the measured spectra could be achieved using the parameters $g=2$, $A=-5.75$ mT$\times g\mu_B$, $D_{001}=-0.1$ mT$\times g\mu_B$, $D_{111}=0.1$ mT$\times g\mu_B$, and $a=-1.55$ mT$\times g\mu_B$. The upper part of Fig. 2 shows the angular dependence of the resonance positions calculated with these parameters,[32] with the size of the dots corresponding to the expected intensity of the resonance lines. The dashed lines in the lower diagram are the EPR spectra obtained from these simulations assuming that the resonances are derivatives of Lorentzian lines with peak-to-peak linewidths of 3.5 mT. Especially the hyperfine splitting at $\varphi=30°$ and $\varphi=90°$ and the fine-structure splitting at $\varphi=0°$ at $\mu_0 H\approx 310-320$ mT and

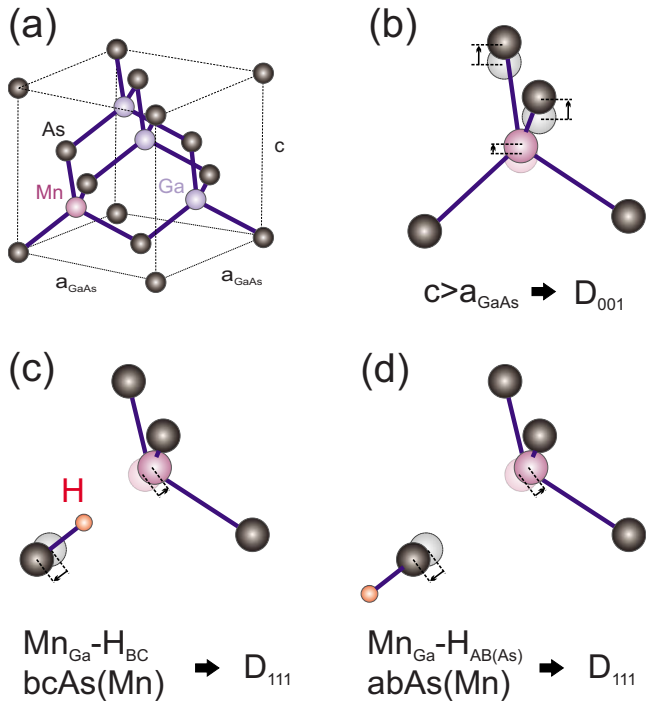

FIG. 4. (Color online) (a) Schematic picture of the $Ga_{1-x}Mn_xAs$ crystal illustrating the origin of the uniaxial crystal-field anisotropy contributions D_{001} and D_{111} in $\mathcal{H}_S$. (b) D_{001} is caused by the uniaxial epitaxial strain ($c > a_{GaAs}$), while the change in local symmetry due to the incorporation of hydrogen is accounted for by D_{111} [(c) and (d)]. In (c) the hydrogen atom is shown in the bond-centered position, denoted as Mn_{Ga}-H_{bc} in Ref. 17 corresponding to bcAs(Mn) in Ref. 16. In (d) the hydrogen atom is shown in the antibonding position, denoted as Mn_{Ga}-$H_{ab(As)}$ in Ref. 17 corresponding to abAs(Mn) in Ref. 16. The arrows indicate a slight shift of the As and the Mn_{Ga} atoms from the substitutional lattice sites.

$\mu_0 H \approx 340-350$ mT are reproduced very well by the simulation. A change in the signs of the parameters in $\mathcal{H}_S$ has only a minor influence on the resulting spectra.

Note that the anisotropic EPR signal of the $Mn^{2+}(3d^5)$ state could only be detected after hydrogenation. In contrast to the compensated $Ga_{1-x}Mn_xAs$ samples of Almeleh and Goldstein[23] and Fedorych *et al.*,[24] our samples did not show an EPR signal in their as-grown state.

The intensities and linewidths of the well-resolved resonances at $\varphi = 30°$ allow an estimation of the $Mn^{2+}(3d^5)$ concentration to 6.0×10^{19} cm$^{-3} = 0.0027 N_0$, where $N_0 = 2.21 \times 10^{22}$ cm^{-3} is the concentration of the cation lattice sites. As usual in EPR, the accuracy of this concentration is about a factor of 2. This value for $[Mn^{2+}(3d^5)]$ is in good agreement with the Mn concentration $[Mn] \approx 0.005 N_0$ determined from the growth parameters, which indicates that after hydrogenation most—if not all—Mn atoms are in the $Mn^{2+}(3d^5)$ state observed in EPR.

The values for the hyperfine splitting A and the cubic anisotropy a agree well with those reported in literature for Mn_{Ga} in GaAs.[23,24] Fedorych *et al.*[24] found for their partially compensated LT-MBE $Ga_{1-x}Mn_xAs$ samples with $10^{-4} < x < 10^{-3}$ a linear dependence of $D_{001} = (96.3x + 0.112)$ mT $\times g\mu_B$ on x. An extrapolation of this behavior into the concentration range of our MOVPE-grown sample ($x = 0.0027$ from EPR) would predict $D_{001} \approx 0.37$ mT $\times g\mu_B$, which is substantially larger than $|D_{001}| = 0.1$ mT $\times g\mu_B$ determined by our simulation. Since the magnitude of the uniaxial crystal-field anisotropy in growth direction is closely related to the compressive strain of the $Ga_{1-x}Mn_xAs$ layer, which in turn depends more on the concentration of defects such as As antisites As_{Ga} and Mn interstitials Mn_I rather than the Mn_{Ga} concentration,[33–37] the small absolute value of D_{001} confirms the high crystalline quality of the MOVPE samples already noted by Hartmann *et al.*[25] For the uniaxial crystal-field anisotropy in the ⟨111⟩ directions D_{111}, we obtain a similar low value by simulation as for D_{001}, indicating that the incorporation of hydrogen also only has a minor influence on the $Mn^{2+}(3d^5)$ electron wave function. In fact, nearly the same level of agreement between the experimentally observed and the simulated EPR spectra is obtained assuming no D_{111} at all. We therefore have to conclude that EPR results indicate that at least the majority of the Mn atoms in the sample with $x \approx 0.005$ are in a Mn^{2+} state after hydrogenation, which is indistinguishable from the Mn^{2+} state obtained by compensation. Since the presence of H in a bond-center configuration—even if relaxed to an off-axis position—would most likely lead to a strong crystal-field anisotropy, we tentatively conclude from the EPR that H is either incorporated in an antibonding position leaving the local geometry and crystal fields at the Mn atom essentially unchanged or that H is rather incorporated as a compensating donor, not forming a complex at all. This finding is supported by XAFS results obtained on the LT-MBE samples as discussed in Secs. V and VI.

Finally, we point out that we have not been able to observe a resolved fine structure in the EPR on hydrogenated LT-MBE grown samples which have a much higher Mn concentration compared to the MOVPE samples. The spectra of the hydrogenated samples rather exhibit a broad resonance with a peak-to-peak linewidth of 65–70 mT at $g = 2.0$ [Fig. 1(b)]. A similarly broad EPR has already been reported in hydrogenated $Ga_{1-x}Mn_xAs$ with $x = 0.07$ by Thevenard *et al.*[12] We suspect that the high Mn concentration of paramagnetic centers leads to an interaction between neighboring Mn^{2+} centers resulting in a broadening that prohibits detection of the fine structure in EPR.

IV. HR-XRD

HR-XRD measurements were performed at $\lambda = 1.540\,595(2)$ Å (Cu $K\alpha_1$ line) using a Philips X'Pert MRD diffractometer equipped with a $4 \times$Ge(220) Bartels primary monochromator. Figure 5(a) shows a reciprocal space map of the asymmetric (404) reflex of a $Ga_{1-x}Mn_xAs$ layer with nominal Mn concentration $x = 0.039$, with the diffracted x-ray intensity plotted as contour lines on a logarithmic scale. The out-of-plane and in-plane reciprocal-lattice vectors $q_\perp$ and $q_\parallel$ are given in units of $4\pi/\lambda$, the "reciprocal-lattice units" (rlu). The most intense reflex at $q_\perp = q_\parallel = 0.545$ rlu is due to the GaAs substrate, while the weaker reflex at the same $q_\parallel = 0.545$ rlu, but smaller $q_\perp = 0.542$ rlu is due to the $Ga_{1-x}Mn_xAs$ layer. The fact that $q_\parallel$ of the $Ga_{1-x}Mn_xAs$ layer

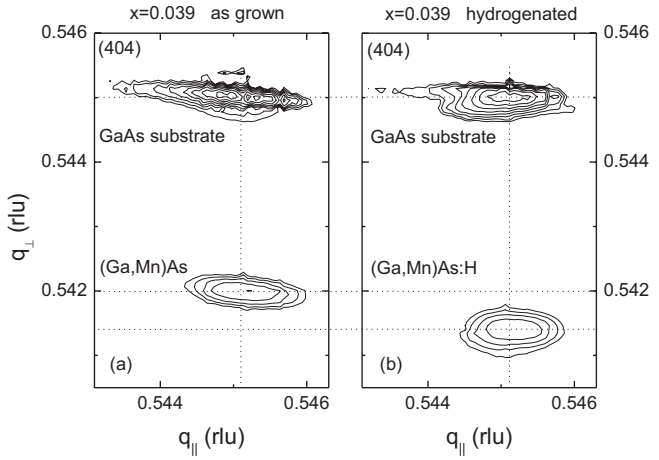

FIG. 5. Reciprocal space map of the asymmetric (404) reflex of a $Ga_{1-x}Mn_xAs$ layer with nominal Mn concentration $x=0.039$ (a) before and (b) after hydrogenation.

is the same as for the GaAs substrate shows that the $Ga_{1-x}Mn_xAs$ film is grown pseudomorphically with the same in-plane lattice parameter $a=2\lambda/q_{\parallel}(\mathrm{rlu})=5.653$ Å on the GaAs substrate. The smaller $q_{\perp}$ corresponds to an enlarged out-of-plane lattice parameter $c=2\lambda/q_{\perp}(\mathrm{rlu})=5.685$ Å perpendicular to the layer caused by compressive strain relaxing in growth direction. The hydrogenated sample in Fig. 5(b) reveals a further enlargement of c by $\Delta c=6\times10^{-3}$ Å, while a remains unchanged.

Having shown that both as-grown and hydrogenated $Ga_{1-x}Mn_xAs$ layers are strained compressively, in the following we will focus on the determination of c via $2\Theta/\Omega$ scans of the symmetric (004) reflex. In this case c can be determined via the Bragg formula $c=2\lambda/\sin\Theta$. Figure 6 compares the $2\Theta/\Omega$ scans of the symmetric (004) reflex of several $Ga_{1-x}Mn_xAs$ layers with varying Mn concentration x before (solid circles) and after (open circles) hydrogenation. Again, the most intense signal at $2\Theta=66.058°$ can be attributed to the (004) reflex of the GaAs substrate, while the peak at lower angle (larger c) corresponds to the (004) reflex of the $Ga_{1-x}Mn_xAs$ layer. There is a clear shift of the peak position of the $Ga_{1-x}Mn_xAs$ (004) reflex to lower 2Θ for increasing x, in agreement with previous investigations.[33,34,38] After hydrogenation we observe an additional shift to smaller 2Θ.

The pronounced interference fringes can be used for the determination of the $Ga_{1-x}Mn_xAs$ layer thickness d. For the samples with $x=0.033$, 0.039, and 0.047 we obtain $d=178$, 263, and 175 nm before and $d=148$, 239, and 155 nm after hydrogenation, respectively, with an accuracy of 10 nm. Consequently, there is a reduction in layer thickness after hydrogenation by 20–30 nm independent of Mn concentration, which we attribute to a steady atomic hydrogen etching during the long-term hydrogenation process.[39] Thus the etching affects only ≈10%–15% of the total sample thickness. Moreover, even if the removal of atoms from the surface could be *a priori* nonstoichiometric, the presence of clear interference fringes in the HR-XRD curves of the hydrogenated samples suggests a high quality of the interfaces, and the defective surface possibly generated upon hydrogenation

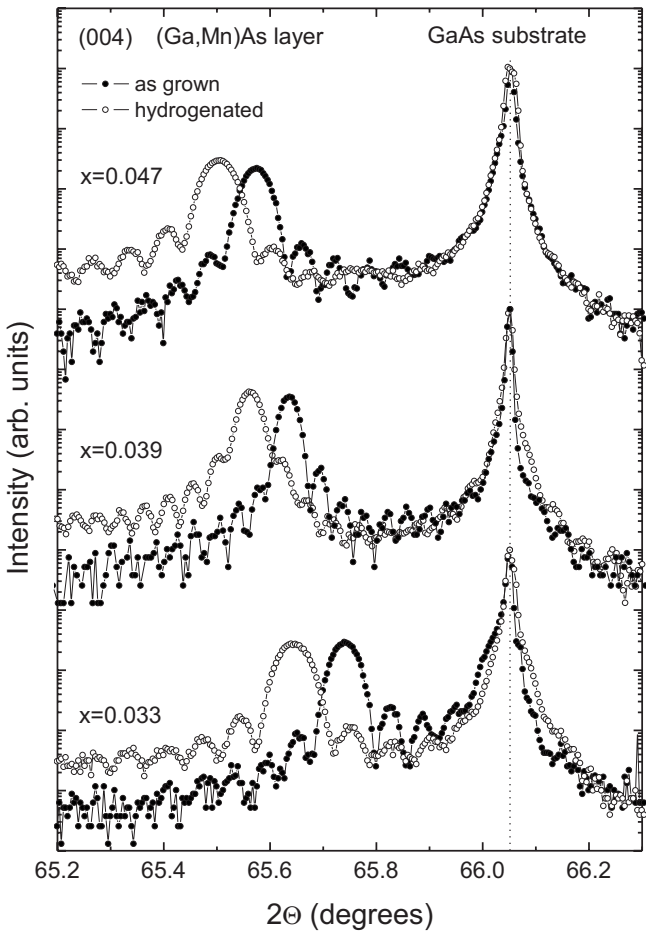

FIG. 6. $2\Theta/\Omega$ scans of the symmetric (004) reflex of $Ga_{1-x}Mn_xAs$ layers with varying Mn concentration x before (solid circles) and after (open circles) hydrogenation. For clarity curves are shifted vertically. The angle $2\Theta=66.058°$ marked by the vertical dashed line corresponds to the (004) reflex of the GaAs substrate.

should extend over a thickness sensibly lower than the etched thickness. As a consequence, the ratio of Mn atoms possibly involved in surface compounds to the total Mn concentration is supposed to be even lower than 10%. Since all measurements presented in this paper probe the whole epilayer or are sensitive to the GaAs lattice structure, the contribution of surface Mn can be neglected for our analyses.

For further analysis we calculate the relaxed lattice parameters of hypothetically unstrained $Ga_{1-x}Mn_xAs$ layers using[40]

$$a_{\mathrm{relax}}=\frac{1-\nu}{1+\nu}c+\frac{2\nu}{1+\nu}a. \tag{2}$$

We assume that $Ga_{1-x}Mn_xAs$ has the same elastic constant as GaAs and, in approximation, use the value $\nu=0.311$ of GaAs (Ref. 41) for the Poisson ratio. The relaxed lattice constants a_{relax} before (solid symbols) and after (open symbols) hydrogenation obtained in this way as a function of x are plotted in Fig. 7(a). The circles correspond to the samples investigated in Fig. 6 and the triangles to the samples further characterized via XAFS below. As already evident from the discussion

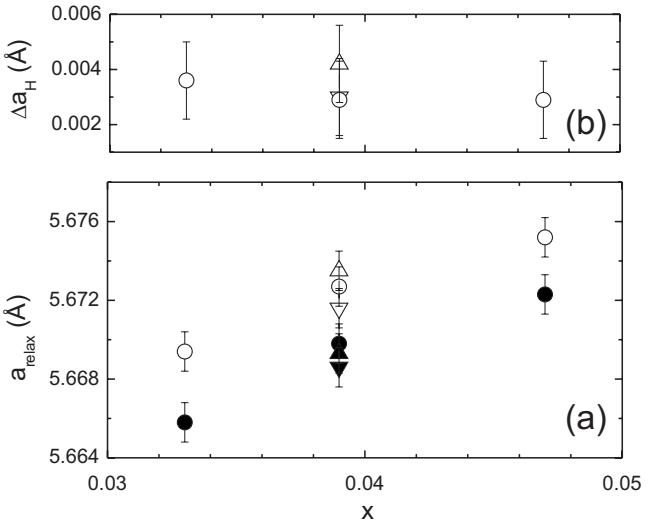

FIG. 7. (a) Relaxed lattice parameter as a function of Mn concentration x before (solid symbols) and after (open symbols) hydrogenation. The circles correspond to the samples investigated in Fig. 6 and the triangles to the samples further characterized via XAFS below. The error bars are deduced from the full width at half maximum of the (004) reflex of the (Ga,Mn)As layer in Fig. 6. (b) Increase in relaxed lattice parameter upon hydrogenation Δa_H. The notation is the same as in (a).

of the $2\Theta/\Omega$ scans, there is an approximately linear increase in a_{relax} with x and an additional increase by $\Delta a_H \approx (3.5 \pm 1.4) \times 10^{-3}$ Å rather independent of x—or even slightly decreasing with increasing x—after hydrogenation [Fig. 7(b)].

The come about of a_{relax} of $Ga_{1-x}Mn_xAs$ thin films is quite complex. Ohno *et al.*[38] proposed a universal Vegard's law with a_{relax} increasing linearly between extrapolated lattice constants of GaAs and MnAs. Schott *et al.*[33] also observed a linear dependence of a_{relax} on the Mn concentration, however with the slope of this linear dependence strongly influenced by the specific growth parameters. Especially the substrate temperature and the As/Ga flux ratio during growth turned out to have strong influence on a_{relax}.[34] Density-functional theory (DFT) calculation by Mašek *et al.* predicts a strong influence of Mn_I interstitial and As_{Ga} antisite defect concentrations on a_{relax}, while the contribution of substitutional Mn_{Ga} concentration was argued to be negligible. Recently, Zhao *et al.*[42] and Daeubler *et al.* showed that though the DFT calculation by Mašek *et al.*[35] strongly underestimated the influence of Mn_{Ga} concentration, the contribution of Mn_I and As_{Ga} concentrations to a_{relax} indeed is important, albeit somewhat smaller than previously thought.

Here, we want to focus on the effect of hydrogenation on the lattice parameter. There already is a non-negligible degree of compensation in the as-grown samples caused by the presence of Mn_I and As_{Ga} defects acting as double donors.[43] For samples grown with similar growth parameters in the same MBE chamber, Daeubler *et al.*[43] observed a slight decrease in the hole concentration from $p \approx 3.2 \times 10^{20}$ cm^{-3} at $x=0.031$ to $p \approx 2.3 \times 10^{20}$ cm^{-3} at $x=0.049$ due to an increasing amount of compensating Mn_I.[43] Hydrogen will most likely only passivate the uncompensated Mn_{Ga} acceptors. Since the concentration of electrically active Mn_{Ga} acceptors in the samples slightly decreases above $x=0.03$, indeed an approximately constant or even decreasing Δa_H would be expected as observed in Fig. 7.

In the following we want to estimate the volume increase ΔV_H of a single Mn_{Ga}-As pair upon hydrogenation via

$$N_0 V_{\text{Mn-As-H}} = N_0 V_{\text{Mn-As}} + [\text{H}]\Delta V_H. \quad (3)$$

Here $V_{\text{Mn-As-H}} = (a_{relax} + \Delta a_H)^3/4$ and $V_{\text{Mn-As}} = a_{relax}^3/4$ are the effective volumes of a single Mn_{Ga}-As-H complex and a single Mn_{Ga}-As pair, respectively, $a_{relax} = 5.67$ Å is the lattice parameter of an as-grown $Ga_{1-x}Mn_xAs$ layer, $N_0 = 2.21 \times 10^{22}$ cm^{-3} is again the volume density of Ga lattice sites, and [H] is the hydrogen concentration. We assume that the increase in lattice parameter $\Delta a_H \approx (3.5 \pm 1.4) \times 10^{-3}$ Å is caused by a hydrogen concentration which approximately equals the hole concentration before hydrogenation $[\text{H}] \approx p \approx (3 \pm 1) \times 10^{20}$ cm^{-3}. From this we obtain $\Delta V_H \approx (6 \pm 3)$ Å^3 and $\Delta V_H / V_{\text{Mn-As}} \approx 0.14 \pm 0.07$. Goss and Bridon[17] calculated for the on-axis bond-centered Mn_{Mn}-H_{bc} complex, a bond-centered complex with the H atom lying considerably off the [111] axis (Mn_{Mn}-H^*_{bc}) [Fig. 8(a)], and the antibonding (Mn_{Mn}-$H_{ab(As)}$) [Fig. 8(b)] configuration values of $\Delta V_H / V_{\text{Mn-As}}(Mn_{Mn}\text{-}H_{bc}) = 0.17$, $\Delta V_H / V_{\text{Mn-As}}(Mn_{Mn}\text{-}H^*_{bc}) = 0.11$, and $\Delta V_H / V_{\text{Mn-As}}(Mn_{Mn}\text{-}H_{ab(As)}) = 0.07$, respectively.

Consequently, our HR-XRD data agree best with the bond-centered configurations. However, also the volume increase expected for the antibonding configuration is in agreement with our results within the error bars. Therefore, our HR-XRD data show that there indeed is a volume increase upon hydrogenation as expected for Mn-H complex formation. But the accuracy of this experimental technique is not sufficient to draw unambiguous conclusions about the specific nature of the Mn-H configuration. A physical quantity that significantly differs for the bond-centered and the antibonding configurations is the corresponding radial distribution function of the Mn atom [Figs. 8(c) and 8(d)]. In the antibonding configuration all four As nearest neighbors have almost the same distance ≈2.5 Å from the Mn atom [Figs. 8(b) and 8(d)], while in the off-axis bond-centered configuration, there is one As atom having a significantly larger distance of ≈3.2 Å [Figs. 8(a) and 8(c)]. An experimental method to study this local structure of the Mn atoms is extended XAFS (EXAFS).

V. EXAFS

XAFS measurements were performed at the European Synchrotron Radiation Facility in Grenoble [beamline BM 29 (Ref. 44)] using a Si (311) monochromator in x-ray fluorescence detection mode. For each of the two samples with $x=0.039$, we investigated an as-grown piece, a hydrogenated piece, and a reference piece, treated in the same way as the hydrogenated one, but with the hydrogen plasma switched off. The energy dependence of the x-ray absorption coefficient $\mu(E)$ at the Mn K edge was measured detecting the intensity of the Mn $K\alpha$ fluorescence line by means of a 13-element Ge hyperpure solid-state detector. Note that we also

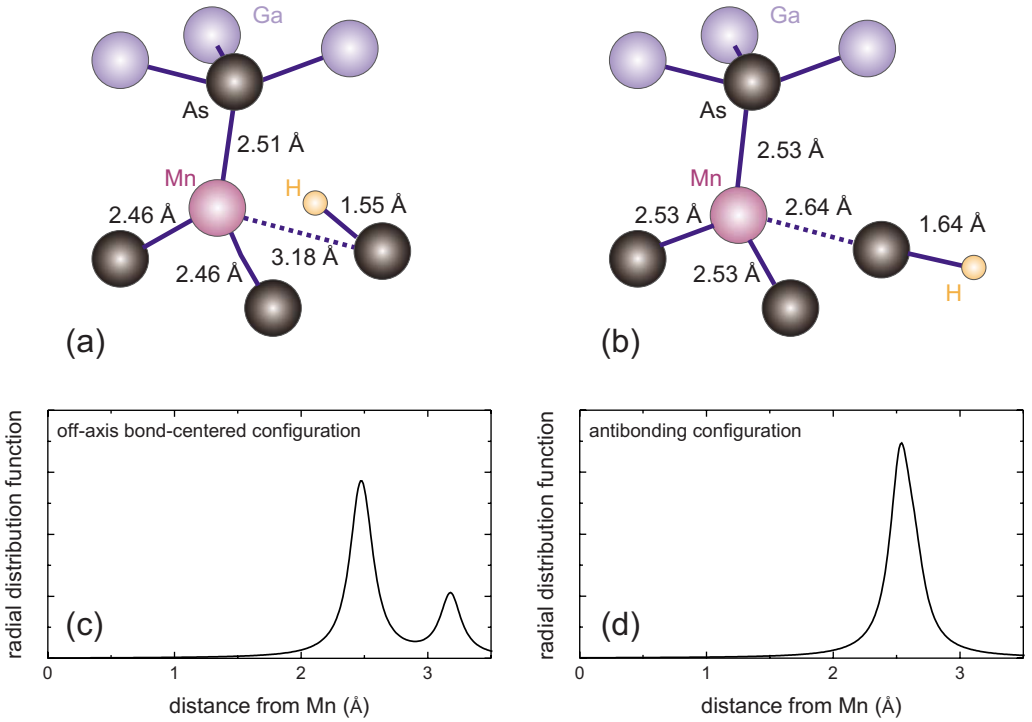

FIG. 8. (Color online) (a) Off-axis bond-centered configuration (Mn_{Mn}-H^{*}_{bc}), and (b) antibonding configuration (Mn_{Mn}-$H_{ab(As)}$) of the Mn_{Ga}-H complex with the bond lengths calculated by Goss and Briddon (Ref. 17). Similar values have been obtained by Bonapasta *et al.* (Ref. 16). (c) Expected radial distribution function for the off-axis bond-centered configuration (Mn_{Ga}-H^{*}_{bc}). (d) Expected radial distribution function for the antibonding configuration (Mn_{Ga}-$H_{ab(As)}$). To estimate these radial distribution functions we used the bond lengths to the neighboring As atoms from Ref. 17 depicted in (a) and (b) and broadened the distribution function by Lorentzians with a full width at half maximum (FWHM) of 0.2 Å.

checked for a possible impact of synchrotron irradiation on sample properties and especially the stability of the Mn-H complexes and in particular verified that the hydrogenated samples showed the characteristic local vibrational mode at 1546 cm^{-1} (note that we used the isotope deuterium), the expected shift of the (004) reflex in HR-XRD, as well as the suppression of ferromagnetic and spin-wave resonances both before and after the XAFS measurements. Nevertheless, the Mn-H complexes could still be dissociated or excited to a higher energy state during the experiment and reform at the end. However, a transient dissociation appears to be highly unlikely considering that the reactivation of Mn acceptors is a very long procedure which requires the samples to be heated to $T>150$ °C for several hours.[9] Furthermore, since EXAFS is highly sensitive to changes in the position of atoms immediately close to the central Mn, an excited state of the H atom in the vicinity of the Mn atom, such as near the bond-center position, would still be detectable by this technique.

The XAFS absorption coefficient $\mu(E)$ of an as-grown $Ga_{1-x}Mn_xAs$ sample with $x=0.039$ is shown in Fig. 9. The sharp rise at $E_0=6539$ eV is the Mn K absorption edge. Above this energy, electrons are excited from the Mn K $1s$ core level into the continuum. In a simple picture[45] the photoelectron with mass m propagates with wave number $k=\sqrt{2m(E-E_0)/\hbar^2}$ and can scatter from the electrons of the neighboring atoms. The photoelectron wave backscattered from the neighbors interferes with the outgoing photoelectron wave and such interference causes oscillations in the absorption coefficient which contain information about the local crystallographic neighborhood of the absorbing Mn atom,[46] which will be extracted in the following.

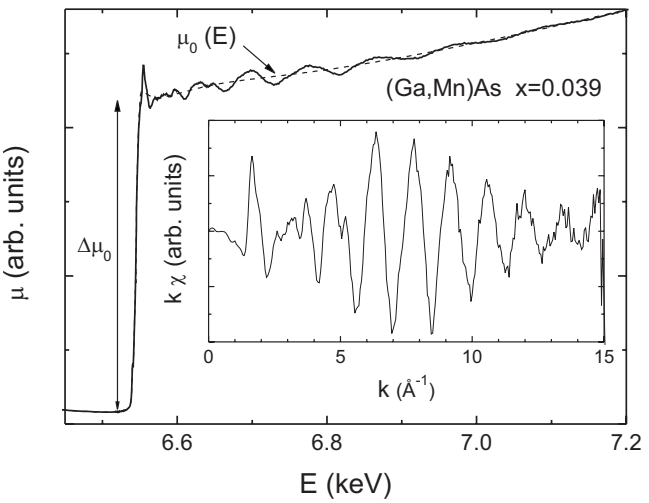

FIG. 9. XAFS absorption coefficient $\mu(E)$ of an as-grown $Ga_{1-x}Mn_xAs$ sample with $x=0.039$. The dashed curve is a smooth background function representing the absorption of an isolated Mn atom $\mu_0(E)$. Inset shows the extracted $k\chi(k)$ spectrum described in the text.

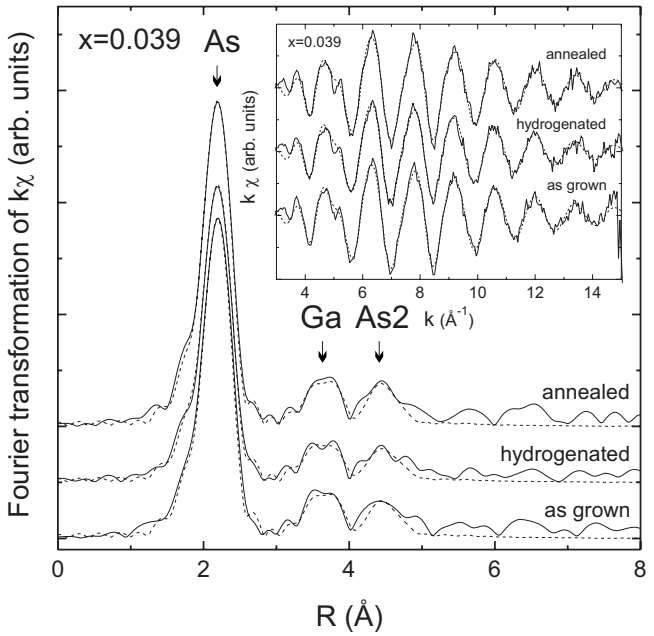

FIG. 10. Comparison of the Fourier transforms of the Mn K-edge EXAFS χ functions of an as-grown, a hydrogenated, and an annealed reference sample. Inset shows the k-weighted Mn K-edge EXAFS χ functions. The dashed curves are fits to the measured data. For clarity the curves are shifted vertically.

The $\mu(E)$ spectrum typically is subdivided into two intervals: the regime within ≈50 eV of the absorption edge and the energy range far above the absorption edge (50–1000 eV). Accordingly, the investigation of the $\mu(E)$ spectrum is called x-ray absorption near-edge spectroscopy (XANES) and extended x-ray absorption fine-structure spectroscopy (EXAFS) depending on the energy range. First we will focus on the EXAFS analysis, while XANES will be discussed in Sec. VI.

The first step in EXAFS data analysis is the subtraction of a smooth background function representing the absorption of an isolated Mn atom $\mu_0(E)$ (dashed curve in Fig. 9). In this way we obtain the EXAFS fine-structure function $\chi(E) = [\mu(E) - \mu_0(E)]/\Delta\mu_0$, where $\Delta\mu_0$ is the jump in $\mu(E)$ at $E = E_0$. The extracted $\chi(k)$ using the AUTOBK code[47] multiplied by k as a weighing function is shown in the inset of Fig. 9.

The same analysis was performed for EXAFS data obtained for the hydrogenated and the annealed reference samples (inset of Fig. 10). In the Fourier transforms of these Mn K-edge EXAFS $k\chi(k)$ functions shown in Fig. 10, the different coordination shells of the zinc-blende lattice surrounding the Mn atom can be distinguished, with peaks at ≈2.2, ≈3.7, and ≈4.4 Å corresponding to the nearest As, nearest Ga, and second-nearest As neighbors, respectively. The Fourier transforms found for the as-grown, hydrogenated, and annealed reference samples are virtually identical, except for a reduced magnitude of the nearest As-neighbor peak around 2.2 Å for the hydrogenated sample. This observation is confirmed by the results of corresponding measurements performed on a set of second samples with same x (not shown).

We performed an *ab initio* modeling of the absorption cross section using a cluster comprising the first three coordination shells of the Mn atom. For the calculation of the theoretical backscattering amplitudes and phase shifts, we used the FEFF 6L.02 code.[48] Subsequently, we fitted the data in R space within a window from 1.5 to 5.2 Å, which includes the first three coordination shells, using the FEFFIT program[49] (dashed lines in Fig. 10). The resulting fitting parameters of the three shells—nearest As-neighbor bond length R_{As}, nearest Ga-neighbor bond length R_{Ga}, and second-nearest As-neighbor bond length R_{As2}, as well as nearest As-neighbor Debye-Waller factor σ^2_{As}, nearest Ga-neighbor Debye-Waller factor σ^2_{Ga}, and second-nearest As-neighbor Debye-Waller factor σ^2_{As2}—are plotted as a function of sample treatment in Fig. 11. There, "H" and "A" denote "hydrogenation" and "annealing with plasma switched off," respectively. Sample 1 is the one already investigated in Fig. 10. The fitting parameters obtained for the as-grown samples are in good agreement with values determined for R_{As}, R_{Ga}, R_{As2}, σ^2_{As}, σ^2_{Ga}, and σ^2_{As2} of $Ga_{1-x}Mn_xAs$ thin films before.[50] The amplitude reduction in the Fourier transform of $k\chi(k)$ after hydrogenation already mentioned above is accounted for by the significant increase in the nearest As-neighbor Debye-Waller factor σ^2_{As} of the hydrogenated sample shown in Fig. 11(d). The fits also indicate an increase in the second and third shell Debye-Waller factors σ^2_{Ga} and σ^2_{As2} for the hydrogenated samples [Figs. 11(e) and 11(f)]. The physical meaning of the Debye-Waller factors' rise is an increase in local structural disorder after hydrogenation. Besides, there seems to be a slight increase in R_{As} after hydrogenation, while R_{Ga} and R_{As2} remain almost unaffected, indicating that Mn and H are at least correlated. Since all parameters of the annealed reference samples within error bars are the same as those of the as-grown samples, a significant effect of the elevated temperature alone during hydrogenation can be excluded.

It is important to mention that we obtained the best fit to the spectra of the hydrogenated samples using the same cluster—with the same distance for all four As nearest neighbors—as for the annealed and the as-grown samples. Especially, a cluster with one As atom of the first shell having a larger distance according to Fig. 8(a) did not improve the fit. This is also obvious from the Fourier transform of $k\chi(k)$ for the hydrogenated sample in Fig. 10. From the—according to DFT calculations[16,17]—energetically most favorable cluster model, the off-axis bond-centered configuration of the hydrogen atom [Fig. 8(a)], we would have expected at least an additional peak or shoulder on the higher distance side of the nearest As-neighbor peak, similar to the additional peak of the first shell in the schematic radial distribution function in Fig. 8(c). The fact that no such second peak or shoulder can be resolved for any of the two hydrogenated samples investigated strongly suggests that the off-axis bond-centered Mn-H complex of Fig. 8(a) predicted by theory is not detectable in our samples with EXAFS. Our measurements rather agree with the one-peak structure of the first coordination shell schematically shown in Fig. 8(d) for the antibonding configuration in Fig. 8(b). Other possibilities which would account for the EXAFS data could be that the H atom is not bound to a nearest As neighbor, but to a more distant As atom or that the H atom is present as a compensating interstitial donor. Both situations would also result in

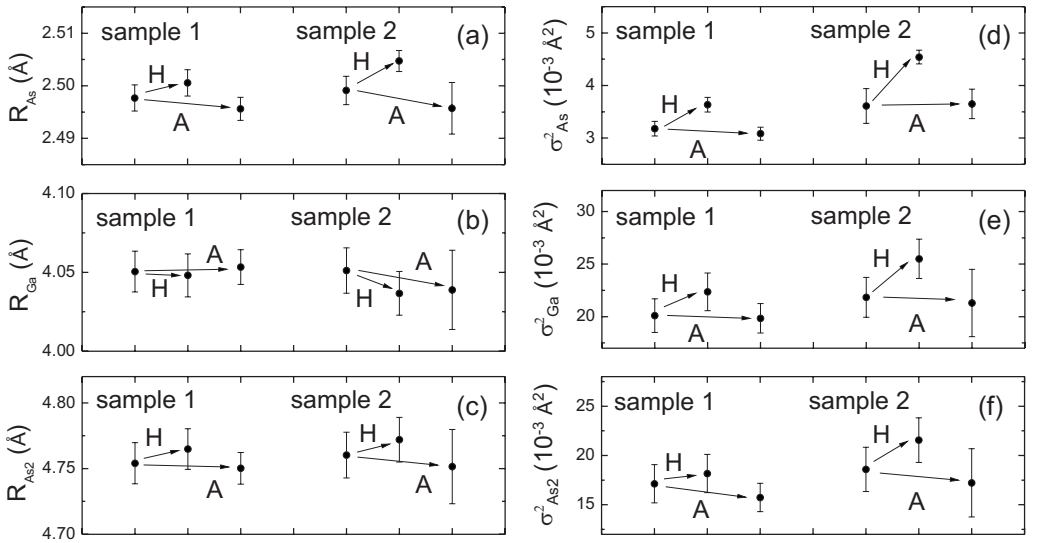

FIG. 11. (a) Nearest As-neighbor bond length R_{As}, (b) nearest Ga-neighbor bond length R_{Ga}, and (c) second-nearest As-neighbor bond length R_{As2}, as well as (d) nearest As-neighbor Debye-Waller factor σ^2_{As}, (e) nearest Ga-neighbor Debye-Waller factor σ^2_{Ga}, and (f) second-nearest As-neighbor Debye-Waller factor σ^2_{As2} as a function of sample treatment (H=hydrogenation, A=annealing) determined from the fits to the spectra on sample 1 in Fig. 10 and on sample 2.

an one-peak structure of the first coordination shell. Note that in this case it would be difficult to attribute a H atom to a specific Mn atom. This is due to the fact that for $x=0.039$ the average Mn-Mn distance is $d_{Mn\text{-}Mn}=10.5$ Å, which corresponds approximately to two lattice constants.

VI. XANES

In this section we will focus on the investigation of the near Mn K edge region of the $\mu(E)$ spectrum. Figure 12 compares the experimental XANES spectra of an as-grown and a hydrogenated piece of sample 2 with *ab initio* simulations performed in the full multiple scattering (FMS) approach assuming the formation of different Mn-H complexes: single Mn (sMn), bond-center (bc), and antibonding (ab) complexes with H linked to either Mn or As, and two more complexes (abAsGa, bcAsGa) where the distance between Mn and H is bigger (cf. Table II in Ref. 16). The atom positions in the clusters used for the FMS simulations have been calculated by DFT in the Hubbard $U(\sigma\text{-GGA}+U)$ approximation.[16] We repeated a 64-atom supercell eight times, translating the positions in order to drive a Mn atom to the center of the cell. The clusters consisted, indeed, of 512 atoms for the single substitutional Mn on Ga (sMn) and 520 atoms for the Mn-H complexes.

FMS simulations of the Mn K-edge XANES were performed by using the FEFF 8.1 code[51] based on Green's function calculations in the complex plane. The code employs a Barth-Hedin formulation for the exchange-correlation part of the potential and the Hedin-Lundqvist self-energy correction; calculation of the potential was performed by using a self-consistent field within a 5 Å radius, a distance that includes the third coordination shell of a central Mn. The FMS radius was fixed to 20 Å in order to enclose all the input atoms without using any extra scattering path. This simulation method has already been demonstrated to be effective for the study of N-H complexes in hydrogenated GaAsN (Ref. 52) and for other dilute nitride semiconductors.[53] In the case of the FMS simulations reported in this paper, the imaginary part of the exchange-correlation potential has been corrected by adding a constant shift equal to 1 eV (i.e., of the same

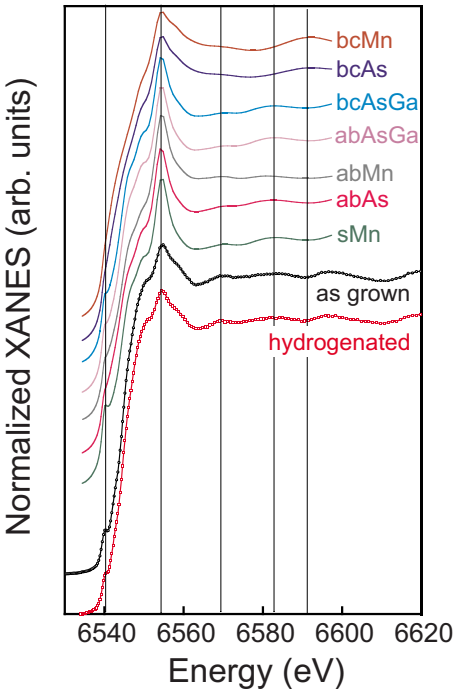

FIG. 12. (Color online) Comparison of the XANES spectra of a hydrogenated and as-grown piece of sample 2 (the two lowest spectra) with *ab initio* simulations performed in the FMS approach for different Mn-H complexes: single Mn (sMn), bond-center (bc), and antibonding (ab) complexes with H linked to either Mn or As, and two more complexes (abAsGa, bcAsGa) where the distance between Mn and H is bigger.

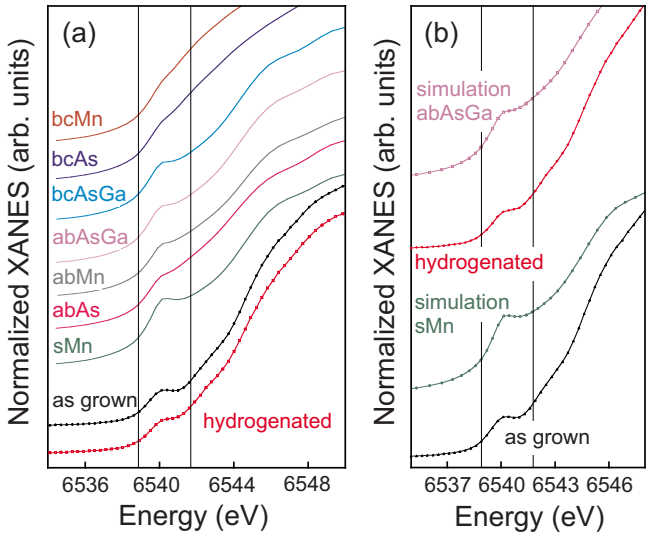

FIG. 13. (Color online) (a) Zoom on the pre-edge region of Fig. 12; the vertical lines delimitate the pre-edge peak/shoulder. (b) Comparison of the experimental XANES spectra with the FMS simulations that give the best agreement, i.e., sMn for the as-grown sample and abAsGa for the hydrogenated one, respectively.

order of the natural width of the Mn K level[54]) to mimic the XANES broadening. In order to obtain an optimal correspondence between experimental data and simulations, the energy scale of calculated spectra has been only slightly shifted (−2.8 eV) and dilated (3%) around the edge position; this has been done based on a comparison between the experimental and theoretical spectra for the untreated $Ga_{1-x}Mn_xAs$ sample, the line shape of which is already well known.[55]

The simulation for Mn_{Ga} (sMn) reproduces the overall experimental spectrum of the as-grown sample and the relative positions of the spectral features well with a pre-edge peak at 6540 eV, a main peak at 6554 eV, weaker peaks at 6570 and 6582 eV (emphasized by vertical lines in Fig. 12), and a valley at 6591 eV. After hydrogenation the pre-edge peak at 6540 eV becomes a shoulder [Fig. 13(a), bottom], while the rest of the spectrum does not change appreciably (Fig. 12). The simulation for the bond-centered complexes (bcMn, bcAs) does not reproduce the experimental spectrum of the hydrogenated sample (absence of the valley at 6563 eV, absence of the peaks at 6570 eV and 6582 eV, and presence of a peak at 6591 eV where a valley is observed experimentally), so that the formation of these complexes can be discarded on the basis of XANES for the samples under study. This is in agreement with the results of the EXAFS data analysis discussed above. Inspecting the simulations for the other Mn-H complexes, a shoulder around 6540 eV (more or less accentuated) is observed in the case of the Mn and the As antibonding complexes (abMn, abAs) and also in the case of the abAsGa and the bcAsGa complexes [Fig. 13(a)]; far from the pre-edge region these simulations are similar to the one for sMn (Fig. 12) and, indeed, well reproduce the experimental spectrum of the hydrogenated sample. Figure 13(b) compares the pre-edge region of the experimental spectra for the untreated and hydrogenated sample 2 with the simulations that yield, for each situation, the best agreement. The fact that we observe only one peak in the pre-edge energy range—and also the fact that the peak is only weakly affected upon hydrogenation—is in agreement with the expectation for magnetic semiconductors with a tetrahedral arrangement of ligands around Mn in the $Mn^{2+}(3d^5)$ configuration.[56]

The XANES results strengthen the conclusion of the EXAFS analysis excluding the formation of the bond-centered complexes in the hydrogenated material studied. Furthermore, the experimental results could be explained again by the formation of either antibonding complexes or other complexes in which the H atom is more distant from the central Mn.

VII. CONCLUSION

In this paper we investigated the changes in the local structure of Mn in $Ga_{1-x}Mn_xAs$ upon hydrogenation in two sets of samples. For diluted samples with $x \approx 0.005$ grown by MOVPE we observed the typical EPR signature of Mn^{2+} ions, the expected oxidation state of Mn in hydrogenated $Ga_{1-x}Mn_xAs$. The uniaxial anisotropy parameter associated with the incorporation of hydrogen atoms $D_{111}=0.1$ mT $\times g\mu_B$ determined from a simulation of the anisotropic EPR signal is very small. Therefore, from EPR it seems that most H atoms occupy positions which do not lead to crystal-field anisotropies at the Mn atom which are easily detectable in EPR. The results obtained with this method favor antibonding positions for H in Mn-H complexes or even the incorporation of H at positions not associated with Mn itself, such as interstitial hydrogen.

Our analysis of the HR-XRD data shows that there indeed is a volume increase in the unit cell upon hydrogenation as expected for Mn-H complex formation. However, the accuracy of this experimental technique is not sufficient to draw unambiguous conclusions about the specific nature of the Mn-H configuration.

The conclusions which can be drawn from the EXAFS and XANES experiments on the samples with high Mn concentration are clearer again and agree with the EPR results. The absence of a second peak or shoulder at the first coordination shell in the radial distribution function determined from the Mn K-edge EXAFS, as well as the comparison of the corresponding XANES spectrum with simulations of several complexes, strongly suggests that the bond-centered complex predicted by DFT calculations is not dominant in our hydrogenated samples. Both EXAFS and XANES spectra can rather be explained by the formation of antibonding complexes or complexes in which the H atom is not bound to a nearest As neighbor, but a more distant As atom.

One particular donor leading to compensation which might be envisaged to form upon hydrogenation is the gallium vacancy V_{Ga} decorated with hydrogen atoms.[57,58] While the characteristic vibrational frequency of this complex would be similar to that of As-H, the donor state of the vacancy requires four hydrogen atoms. Although SIMS data have to be interpreted with care, a hydrogen concentration four times larger than the Mn concentration required for a full compensation by H_4-V_{Ga} is at variance with the SIMS

results.[5] However, very little is known about vacancies in $Ga_{1-x}Mn_xAs$ and it would certainly be worthwhile to study the material, e.g., by positron annihilation and further theoretical calculations.

How can the EPR, EXAFS, and XANES results be reconciled with the existing theoretical understanding in particular with respect to the local vibrational mode which is also observed in the LT-MBE grown samples studied here? One obvious difference between the samples traditionally studied with local vibrational mode spectroscopy and those investigated here is the high concentration of dopants and hydrogen atoms in our case. This will most likely lead to interactions between neighboring complexes, already invoked as a possible reason for the failure to observe resolved EPR in the LT-MBE grown material. This interaction could lead to bond-centered complexes not being energetically favored any more at high concentrations. Indeed, also the theoretical calculations predicting the behavior of H in semiconductors are now carried out in large supercells usually containing a single impurity and are therefore more relevant to very dilute systems rather than the high-concentration material studied here. To elucidate this point, a very detailed study varying the Mn and H concentrations and quantitatively comparing, e.g., the Fourier transformation infrared (FTIR) spectroscopy absorption strength and the EPR signal intensity should be carried out, which is beyond the scope of this initial study. Furthermore, the question whether compensation or passivation is taking place when the H atoms are not positioned closely to the Mn atoms should be investigated by thermopower[59] or mobility measurements[60] on samples which are semiconducting both in the as-grown as well as in the hydrogenated state. Finally, ferromagnetic semiconductors are known to be inhomogeneous, so that it could be envisaged that complexes with large distances between Mn and H are formed in regions with high Mn content, dominating the EPR and EXAFS measurements, while well defined complexes with small distances are formed in regions with low concentrations, as predicted by theory. Nevertheless, the present study expands the techniques available for the investigation of the structural effects of hydrogenation on semiconductors.

ACKNOWLEDGMENTS

The work at the Walter Schottky Institut was supported by Deutsche Forschungsgemeinschaft through SFB 631. We acknowledge the ESRF for the provision of beamtime through Project No. HS2726, as well as S. Pasternak and F. Perrin for technical assistance during the XAFS experiment.

*christoph.bihler@wsi.tum.de

[1] H. Ohno, A. Shen, F. Matsukura, A. Oiwa, A. Endo, S. Katsumoto, and Y. Iye, Appl. Phys. Lett. **69**, 363 (1996).
[2] Y. Ohno, D. K. Young, B. Beschoten, F. Matsukura, H. Ohno, and D. D. Awschalom, Nature (London) **402**, 790 (1999).
[3] T. Dietl, H. Ohno, and F. Matsukura, Phys. Rev. B **63**, 195205 (2001).
[4] C. Bihler, M. Althammer, A. Brandlmaier, S. Geprägs, M. Weiler, M. Opel, W. Schoch, W. Limmer, R. Gross, M. S. Brandt, and S. T. B. Goennenwein, Phys. Rev. B **78**, 045203 (2008).
[5] S. T. B. Goennenwein, T. A. Wassner, H. Huebl, M. S. Brandt, J. B. Philipp, M. Opel, R. Gross, A. Koeder, W. Schoch, and A. Waag, Phys. Rev. Lett. **92**, 227202 (2004).
[6] R. Bouanani-Rahbi, B. Clerjaud, B. Theys, A. Lemaitre, and F. Jomard, Physica B **340-342**, 284 (2003).
[7] S. T. B. Goennenwein, T. A. Wassner, H. Huebl, A. Koeder, W. Schoch, A. Waag, J. B. Philipp, M. Opel, R. Gross, M. Stutzmann, and M. S. Brandt, Adv. Solid State Phys. **44**, 453 (2004).
[8] M. S. Brandt, S. T. B. Goennenwein, T. A. Wassner, F. Kohl, A. Lehner, H. Huebl, T. Graf, M. Stutzmann, A. Koeder, W. Schoch, and A. Waag, Appl. Phys. Lett. **84**, 2277 (2004).
[9] L. Thevenard, L. Largeau, O. Mauguin, A. Lemaitre, and B. Theys, Appl. Phys. Lett. **87**, 182506 (2005).
[10] C. Bihler, M. Kraus, M. S. Brandt, S. T. B. Goennenwein, M. Opel, M. A. Scarpulla, R. Farshchi, D. M. Estrada, and O. Dubon, J. Appl. Phys. **104**, 013908 (2008).
[11] C. G. Van de Walle and J. Neugebauer, Nature (London) **423**, 626 (2003).
[12] L. Thevenard, L. Largeau, O. Mauguin, A. Lemaitre, K. Khazen, and H. J. von Bardeleben, Phys. Rev. B **75**, 195218 (2007).
[13] R. Farshchi, P. D. Ashby, D. J. Hwang, C. P. Grigoropoulos, R. V. Chopdekar, Y. Suzuki, and O. D. Dubon, Physica B **401-402**, 447 (2007).
[14] R. Farshchi, O. D. Dubon, D. J. Hwang, N. Misra, C. P. Grigoropoulos, and P. D. Ashby, Appl. Phys. Lett. **92**, 012517 (2008).
[15] R. Rahbi, B. Pajot, J. Chevallier, A. Marbeuf, R. C. Logan, and M. Gavand, J. Appl. Phys. **73**, 1723 (1993).
[16] A. A. Bonapasta, F. Filippone, and P. Giannozzi, Phys. Rev. B **72**, 121202(R) (2005).
[17] J. P. Goss and P. R. Briddon, Phys. Rev. B **72**, 115211 (2005).
[18] P. M. Williams, G. D. Watkins, S. Uftring, and M. Stavola, Phys. Rev. Lett. **70**, 3816 (1993).
[19] M. Höhne, U. Juda, Y. V. Martynov, T. Gregorkiewicz, C. A. J. Ammerlaan, and L. S. Vlasenko, Phys. Rev. B **49**, 13423 (1994).
[20] P. T. Huy and C. A. J. Ammerlaan, Phys. Rev. B **66**, 165219 (2002).
[21] C. Glover, M. E. Newton, P. Martineau, D. J. Twitchen, and J. M. Baker, Phys. Rev. Lett. **90**, 185507 (2003).
[22] S. Ohya, K. Ohno, and M. Tanaka, Appl. Phys. Lett. **90**, 112503 (2007).
[23] N. Almeleh and B. Goldstein, Phys. Rev. **128**, 1568 (1962).
[24] O. M. Fedorych, E. M. Hankiewicz, Z. Wilamowski, and J. Sadowski, Phys. Rev. B **66**, 045201 (2002).
[25] T. Hartmann, S. Ye, P. J. Klar, W. Heimbrodt, M. Lampalzer, W. Stolz, T. Kurz, A. Loidl, H. A. Krug von Nidda, D. Wolverson, J. J. Davies, and H. Overhof, Phys. Rev. B **70**, 233201 (2004).
[26] W. Limmer, A. Koeder, S. Frank, V. Avrutin, W. Schoch, R. Sauer, K. Zuern, J. Eisenmenger, P. Ziemann, E. Peiner, and A.

Waag, Phys. Rev. B **71**, 205213 (2005).
[27] X. Liu and J. K. Furdyna, J. Phys.: Condens. Matter **18**, R245 (2006).
[28] S. T. B. Goennenwein, T. Graf, T. Wassner, M. S. Brandt, M. Stutzmann, J. B. Philipp, R. Gross, M. Krieger, K. Zuern, P. Ziemann, A. Koeder, S. Frank, W. Schoch, and A. Waag, Appl. Phys. Lett. **82**, 730 (2003).
[29] S. T. B. Goennenwein, T. Graf, T. Wassner, M. S. Brandt, M. Stutzmann, A. Koeder, S. Frank, W. Schoch, and A. Waag, J. Supercond. **16**, 75 (2003).
[30] J. Schneider, U. Kaufmann, W. Wilkening, M. Baeumler, and F. Köhl, Phys. Rev. Lett. **59**, 240 (1987).
[31] Y. Tanabe and S. Sugano, J. Phys. Soc. Jpn. **9**, 753 (1954).
[32] T. Graf, M. Gjukic, M. Hermann, M. S. Brandt, M. Stutzmann, and O. Ambacher, Phys. Rev. B **67**, 165215 (2003).
[33] G. M. Schott, W. Faschinger, and L. W. Molenkamp, Appl. Phys. Lett. **79**, 1807 (2001).
[34] G. M. Schott, G. Schmidt, G. Karczewiski, and L. W. Molenkamp, Appl. Phys. Lett. **82**, 4678 (2003).
[35] J. Mašek, J. Kudrnovský, and F. Máca, Phys. Rev. B **67**, 153203 (2003).
[36] I. Kuryliszyn-Kudelska, J. Z. Domagala, T. Wojtowicz, X. Liu, E. Lusakowska, W. Dobrowolski, and J. K. Furdyna, J. Appl. Phys. **95**, 603 (2004).
[37] J. Sadowski and J. Z. Domagala, Phys. Rev. B **69**, 075206 (2004).
[38] H. Ohno, A. Shen, F. Matsukura, A. Oiwa, A. Endo, S. Katsumoto, and Y. Iye, Appl. Phys. Lett. **69**, 363 (1996).
[39] J. W. Elzey, P. F. A. Meharg, and A. Ogryzlo, J. Appl. Phys. **77**, 2155 (1995).
[40] H. Ohno, in *Semiconductor Spintronics and Quantum Computation*, edited by D. D. Awschalom, D. Loss, and N. Samarth (Springer, Berlin, 2002), p. 1.
[41] R. P. Campion, K. W. Edmonds, L. X. Zhao, K. Y. Wang, C. T. Foxon, B. L. Gallagher, and C. R. Staddon, J. Cryst. Growth **251**, 311 (2003).
[42] L. X. Zhao, C. R. Staddon, K. Y. Wang, K. W. Edmonds, R. P. Campion, B. L. Gallagher, and C. T. Foxon, Appl. Phys. Lett. **86**, 071902 (2005).
[43] J. Daeubler, M. Glunk, W. Schoch, W. Limmer, and R. Sauer, Appl. Phys. Lett. **88**, 051904 (2006).
[44] A. Filipponi, M. Borowski, D. T. Bowron, S. Ansell, A. D. Cicco, S. D. Panfilis, and J. P. Itié, Rev. Sci. Instrum. **71**, 2422 (2000).
[45] M. Newville, http://cars9.uchicago.edu/xafs/xas_fun/xas_fundamentals.pdf, 2004.
[46] P. A. Lee, P. H. Citrin, P. Eisenberger, and B. M. Kincaid, Rev. Mod. Phys. **53**, 769 (1981).
[47] M. Newville, P. Livins, Y. Yacoby, J. J. Rehr, and E. A. Stern, Phys. Rev. B **47**, 14126 (1993).
[48] J. J. Rehr, J. Mustre de Leon, S. I. Zabinsky, and R. C. Albers, J. Am. Chem. Soc. **113**, 5135 (1991).
[49] M. Newville, B. Ravel, D. Haskel, J. J. Rehr, E. A. Stern, and Y. Yacoby, Physica B **208-209**, 154 (1995).
[50] Y. L. Soo, G. Kioseoglou, S. Kim, X. Chen, H. Luo, Y. H. Kao, H.-J. Lin, H. H. Hsieh, T. Y. Hou, C. T. Chen, Y. Sasaki, X. Liu, and J. K. Furdyna, Phys. Rev. B **67**, 214401 (2003).
[51] A. L. Ankudinov, B. Ravel, J. J. Rehr, and S. D. Conradson, Phys. Rev. B **58**, 7565 (1998).
[52] G. Ciatto, F. Boscherini, A. A. Bonapasta, F. Filippone, A. Polimeni, and M. Capizzi, Phys. Rev. B **71**, 201301(R) (2005).
[53] G. Ciatto, J.-C. Harmand, F. Glas, L. Largeau, M. Le Du, F. Boscherini, M. Malvestuto, L. Floreano, P. Glatzel, and R. A. Mori, Phys. Rev. B **75**, 245212 (2007).
[54] M. O. Krause and J. H. Oliver, J. Phys. Chem. Ref. Data **8**, 329 (1979).
[55] F. d'Acapito, G. Smolentsev, F. Boscherini, M. Piccin, G. Bais, S. Rubini, F. Martelli, and A. Franciosi, Phys. Rev. B **73**, 035314 (2006).
[56] A. Titov, X. Biquard, D. Halley, S. Kuroda, E. Bellet-Amalric, H. Mariette, J. Cibert, A. E. Merad, G. Merad, M. B. Kanoun, E. Kulatov, and Yu. A. Uspenskii, Phys. Rev. B **72**, 115209 (2005).
[57] A. Amore Bonapasta and M. Capizzi, Phys. Rev. B **61**, 8180 (2000).
[58] A. Janotti, S.-H. Wei, S. B. Zhang, S. Kurtz, and C. G. Van de Walle, Phys. Rev. B **67**, 161201(R) (2003).
[59] M. S. Brandt, P. Herbst, H. Angerer, O. Ambacher, and M. Stutzmann, Phys. Rev. B **58**, 7786 (1998).
[60] N. M. Johnson, R. D. Burnham, R. A. Street, and R. L. Thornton, Phys. Rev. B **33**, 1102 (1986).